ELSEVIER

International Journal of Heat and Fluid Flow 20 (1999) 374–384

International Journal of HEAT AND FLUID FLOW

www.elsevier.com/locate/ijhff

Heat transfer characteristics of shrouded longitudinal ribs in turbulent forced convection

S. Naik [a,*], S.D. Probert [b], I.G. Bryden [a]

[a] *Fluids and Environment Research Group, The Robert Gordon University, School of Mechanical and Offshore Engineering, Schoolhill, Aberdeen AB9 1FR, UK*

[b] *Department of Applied Energy, School of Mechanical Engineering, Cranfield University, Bedford MK43 0AL, UK*

Received 25 November 1997; accepted 6 February 1999

Abstract

Augmenting the heat transfer rates in the internal flow passages of several components of a gas turbine, such as the turbine blades, vanes and combustor walls is an important pre-requisite for maintaining their structural integrity. This is particularly paramount when higher turbine inlet temperatures and pressure ratios are utilised for enhancing the thermal efficiencies of the gas turbine plant. In this study, the heat transfer enhancement, which can be achieved by longitudinal ribs in a variable geometry duct, has been examined. With the base of the ribs maintained at a constant temperature, it was observed that the optimal rib spacing, which corresponded to the maximum heat transfer from the ribs, was a strong function of the rib height to length ratio and the Reynolds number but relatively insensitive to the amount of clearance above the ribs. A design correlation is proposed which shows the distribution of this optimal rib spacing for a wide range of rib geometrical and operational conditions. Comparisons of the longitudinal ribs with pin fin arrays indicated that at rib height to length ratios of $\geqslant 0.24$, higher heat transfers can be achieved with the longitudinal ribs. The frictional characteristics of the longitudinal ribs is comparable to those of circular pin fins. Measurements of the local heat transfer coefficient for the rib surfaces indicate that it is highly non-uniform along the rib height and length and also significantly influenced by the amount of clearance above the ribs. For all the cases examined, it was observed that developing flow conditions (thermally and hydrodynamically) were prevalent within the longitudinal rib channels.

Keywords: Forced convection; Ribs; Shrouds; Thermal optimisation; Gas turbines; Heat exchangers

Notation

A	array base area
A_{ff}	free-flow area
A_s	total surface area of ribs and spacer bars
C	vertical clearance between rib tips and horizontal shroud
D_e	hydraulic diameter based on free flow area and wetted perimeter of the ribs, spacer bars and the enclosed duct
D_h	hydraulic diameter based on free flow area and heated perimeter of ribs and spacer bars
f	Darcy friction factor
h	local rib heat transfer coefficient
h_{av}	average rib array heat transfer coefficient (based on A_s)
H	rib height
k	thermal conductivity of air
L	rib length
m	air mass flowrate
Nu_H	average Nusselt number based on rib height
Nu_d	average Nusselt number based on hydraulic diameter
Nu_{DH}	Nusselt number based on hydraulic diameter of an equivalent empty duct
P	perimeter of ribs, spacer bars and enclosing duct
P_h	perimeter of heated ribs and spacer bars
Pr	Prandtl number
ΔP	total pressure drop of rib array
Q	total heat transfer rate from ribbed array
Re	Reynolds number
s	rib spacing
s_{opt}	optimal rib spacing
t	rib thickness
T^+	non-dimensionalised temperature
T	local fluid temperature within rib channels
T_B	temperature at the base of the ribs
T_{bulk}	bulk fluid temperature
V_{bulk}	bulk fluid velocity
V	local fluid velocity within rib channels
V_0	mean fluid velocity in test duct upstream of the rib array

* Corresponding author. ABB Power Generation Ltd., CH-5407, Baden, Switzerland. Tel.: +41 56 205 4187; fax: +41 56 205 4690

0142-727X/99/$ – see front matter
PII: S0142-727X(99)00022-3

V_{vol}	volume occupied by pins or ribs
V^0_{vol}	volume occupied by an equivalent empty duct
x	distance from rib surface parallel to rib spacing
y	distance from rib base parallel to rib height
z	streamwise distance parallel to rib length
ρ	fluid density
μ	fluid dynamic viscosity
η^+	non-dimensionalised normal distance from rib wall ($= x\rho V_{bulk}\sqrt{f/8}/\mu$)

1. Introduction

The augmentation of the rate of heat transfer in single-phase internal flow systems has received extensive interest over the years due to the wide range of its application in industrial flows. Some of the specific applications include gas turbine blade cooling, compact heat exchangers and more recently electronic cooling. Usually, heat transfer augmentation in these applications is achieved by the utilisation of several devices ranging from bluff body configurations for promoting local turbulence levels to various shapes and sizes of extended surfaces. In gas turbine applications, the heat removal from several components of the unit, such as turbine blades, combustor walls and turbine discs, is an important pre-requisite for maintaining their structural integrity. This has become more paramount in recent years as higher turbine inlet temperatures and pressure ratios are utilised for enhancing the overall thermal efficiency of the gas turbine. Unfortunately, the use of higher inlet temperatures also poses cooling problems, in that the available temperature gradient between the coolant and the component is also reduced.

Pin fins, as turbulence promoters, are commonly employed for the cooling of turbine blades and vanes with which relatively high heat transfer augmentation can be achieved, VanFossen (1982), Brigham and VanFossen (1984), Metzger et al. (1984), Chyu (1990), Minakami et al. (1994) and Babas'haq et al. (1995). Recently Chyu et al. (1996), examined the effect of using in-line and staggered cubic and diamond pin fins. From measurements of the local and average thermal-hydraulic characteristics of such pins, it was found that staggered cubic pins gave much higher heat transfer enhancement compared to the circular pins. However, correspondingly higher pressure losses also ensued with the cubic and diamond pins.

When cooling the central section of the blades, small transverse ribs are commonly employed. Heat transfer in such configurations is achieved by turbulence promotion. The effects of rib spacing and height and the corresponding distribution of the local and average heat transfer coefficients have also been widely reported, e.g. Hishida (1996), Rau et al. (1996), Han and Zhang (1992), and Han et al. (1985).

The present investigation differs from these previous investigations in that the array employed in this study consists of longitudinal, rectangular ribs (i.e. parallel to the mean flow) whose base is at a constant temperature. The rib array is surrounded by a variable geometry adiabatic duct. Previous studies by Naik et al., 1987a, 1988 have shown that for such configurations thermal optimisation (corresponding to the maximum heat transfer rate from the rib array) can be achieved at a specific rib spacing (i.e. the optimal spacing), which is a function of the rib height, length, the amount of clearance above the ribs and the Reynolds number. Optimal rib spacings have also been observed when only natural convection heat transfer occurs from the longitudinal ribs and when they are mounted on a horizontal base, Naik et al. (1987b) or a vertical base Leung et al. (1987). Maximum heat transfer and corresponding optimal rib spacings have also been determined analytically by Bejan and Scuibba (1992) for parallel plates with laminar fully developed flows and by Knight et al. (1991) for longitudinal microchannel ribs. More recently shrouded longitudinal ribs have been examined by Thombre and Sukhatme (1995) and previously by Sparrow et al. (1978), Kadle and Sparrow (1986) and Sparrow and Beckley (1981). The latter studies considered a very limited range of geometrical conditions and thermal optimisation of the rib arrays was not observed.

2. Experimental investigation

2.1. Test facility and instrumentation

The experimental tests with the longitudinal ribs were conducted in a purpose built heat exchanger test facility shown by Fig. 1 for the range of parameters indicated by Table 1. The width of the wind tunnel was 0.24 m and the height of the tunnel was adjustable to a height ($C + H$), with C being a variable such that $0 < C < 90$ mm and H is the rib height. This variability in the tunnel height was achieved by a vertically movable roof section, which was supported externally by two U-beam column sections. A linear traversing mechanism was incorporated into the support columns which allowed vertical displacements of the roof to within 1 mm. Rubber sealing was used between the roof section and the vertical walls of the tunnel to minimise air leakages.

The wind tunnel, which was operated in the suction mode, supplied atmospheric air to the test section by a single-stage centrifugal fan. Air exhausting from the test section is then passed through an insulated mixing chamber, which consisted of two resin-impregnated cardboard honeycombes (65% and 85% porosity) mounted transverse to the mean flow. A number of vertically traversable hypodermic thermocouple probes were located at the outlet of the mixing chamber, where a complete cross-sectional outlet temperature traverse was undertaken for each test. At the same locations, the mean outlet velocities were also measured with several vertically traversable fine pitot-static tubes. These measurements facilitated the evaluation of the bulk mean outlet temperature. A similar procedure was adopted at the inlet to the test section for the evaluation of the mean inlet velocities and the bulk mean inlet temperatures.

The pressure drop within the test section was measured by 16 brass static-pressure tapps, which were installed in the roof of the test section as shown by Fig. 2(b). Details of the pressure drop measurements are indicated by Naik et al. (1988).

The tested longitudinal ribs (Fig. 2(b)) were constructed from a combination of 3 mm thick duralumin ribs and spacer bars, of thermal conductivity 164 W/mK, which are appropriately bolted together so as to form a rigid sandwich. The array was mounted on a duralumin base-plate, 20 mm thick at the rear of which several heating elements, each rated at 400 W for 240 V a.c. are fixed.

Each of the heating elements could be independently controlled, so that either a constant temperature or a constant heat flux boundary condition could be utilised. In this study a constant temperature boundary condition was adopted. A heat-sink compound, of high thermal conductivity, was used to ensure good thermal contact ensued between the ribs, the heating elements and the base plate. This combination produced a temperature difference between the upper surface of the base plate and the roots of the ribs of less than 0.2°C, and a base-temperature which could be maintained constant to within ±0.5°C. The steady-state temperatures of the rib base were indicated by means of 12 thermojunctions, which were

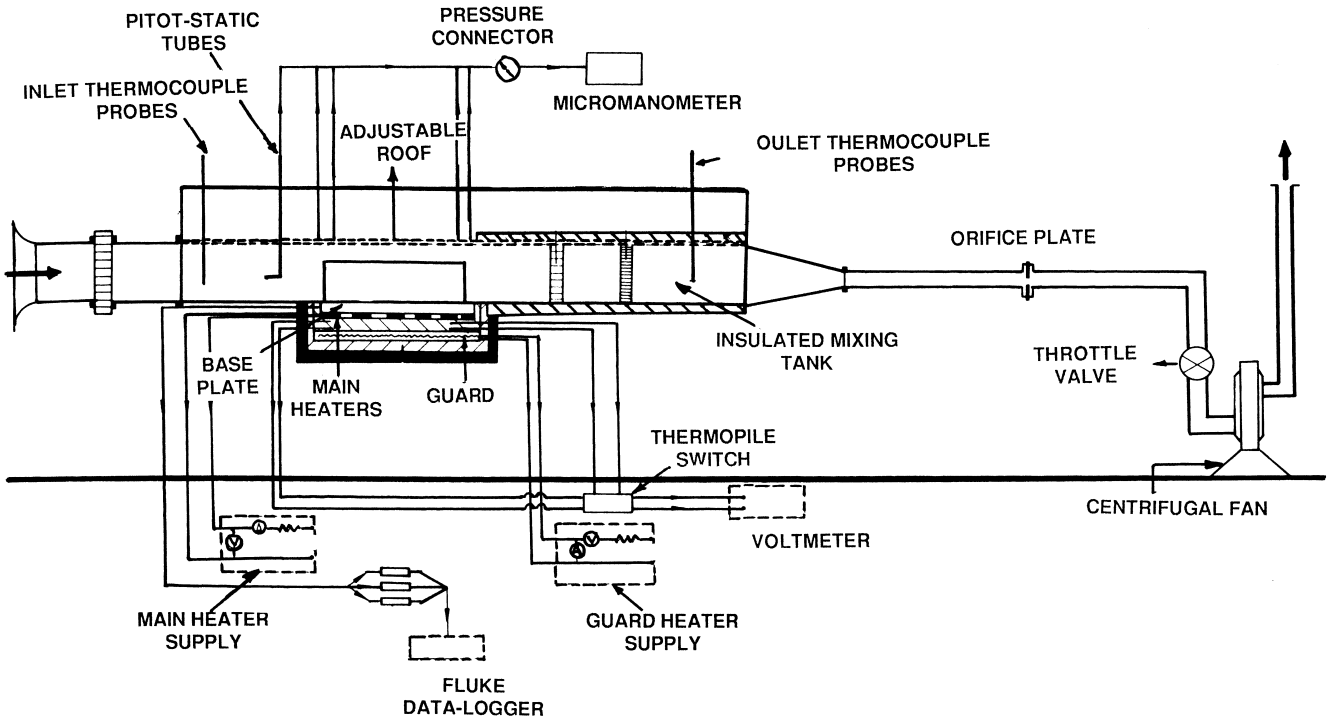

Fig. 1. Experimental test facility and instrumentation.

embedded in the base-plate and located 1 mm below the base of the ribs. An additional 15 thermocouples were located in 2 mm wide by 1.5 mm deep horizontal slotted grooves, (i.e. along anticipated isotherms) within the ribs and held in position by the grooves being packed with a cold-casting aluminum cement, the excess of which when hard was machined off and the surfaces polished flat. The rib embedded thermocouples are not exposed to the air stream as shown by Fig. 2(c).

2.2. Local temperature and velocity measurements

The local velocity distributions within the longitudinal rib passages were measured with a DISA hot-wire anemometer consisting of a 1.25 mm prong width and a 5 μm platinum plated tungsten wire sensor. The local air temperatures were determined with a 0.25 mm copper-constantan hypodermic thermocouple probe. All local mean air-velocity measurements were undertaken within one of the central rib channels and when no heat transfers occurred from the fin-array, so that the hot-wire system could be operated in the constant temperature mode. A schematic diagram of the hot-wire system, its associated instrumentation and the experimental set-up is shown in Fig. 3. The local mean velocities and temperatures were measured at a constant Reynolds number of 1.38×10^4 (as defined by Eq. (2)) and for two rib configurations at $s/t = 1.67$ and 3.33 when $H/L = 0.13$ and $C/H = 0$ or 0.5. Within the central section of the rib channel, measurements were undertaken at several intervals across the width of the channel (i.e. parallel to the rib spacing). These measurements were repeated at several locations along the rib height and at streamwise locations of $z/L = 0.5$ and 0.97 along the rib channel length for the 250 mm long ribs.

Table 1
Ranges of values employed for the experimental parameters

Parameter	Value
Rib spacing to height ratio, s/H	$0.039 \rightarrow 0.6$
Rib length to spacing ratio, L/s	$13 \rightarrow 107$
Rib clearance to height ratio, C/H	$0 \rightarrow 1$
Rib height to length ratio, H/L	$0.085 \rightarrow 0.36$

2.3. Experimental error analysis

Uncertainty and sensitivity analysis has been used for all the average and local measurements of velocities, temperatures and heat fluxes and in the determination of the Reynolds and Nusselt numbers and friction factors. The method used is that recommended by Kline and McClintock (1958) and Moffat (1988). The uncertainty of these parameters are represented in percentages and for the local heat transfer coefficient measurements, error bars are indicated in the appropriate figures.

3. Average thermal-hydraulic characteristics

3.1. Optimal rib spacings

For all the geometrical and operational cases shown in Table 1, previous tests on the ribs considered in this study have shown that maximisation of the steady rate of heat transfer was achievable with respect to variations in the rib spacing, (Naik et al., 1987a, 1988 and Fig. 4). Qualitatively similar graphs to Fig. 4 were obtained for the whole range of geometrical conditions shown in Table 1 and are indicated by Naik et al. (1988). In general it was observed that increasing the rib length results in a reduction of the heat transfer but an increase in the optimal spacing, whereas increasing the rib height increases both the optimal spacing and the heat transfer. The C/H ratio had little or no effect on the optimal spacing but lower heat transfer rates were obtained from the rib configurations when the C/H ratio is increased from zero to unity.

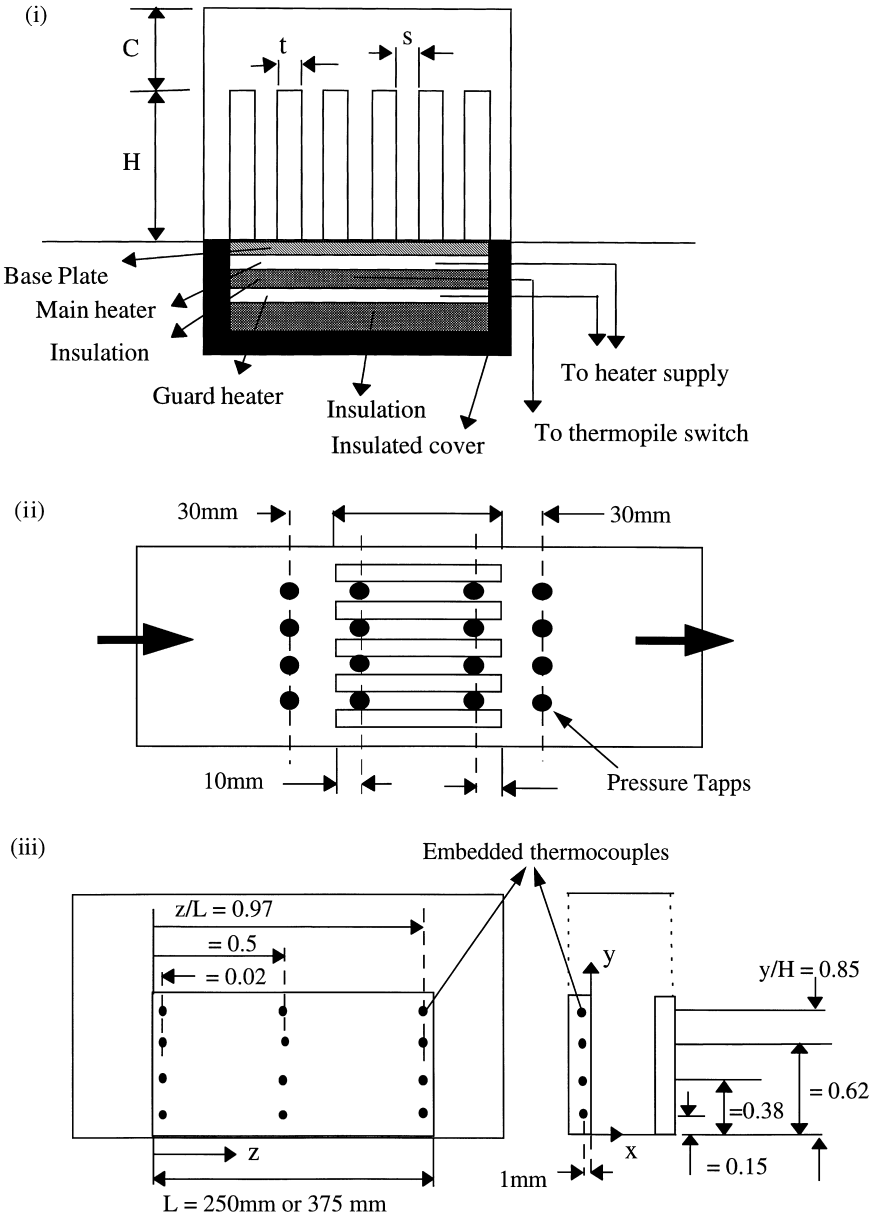

Fig. 2. Experimental details of (i) ribs and heater arrangement, (ii) pressure tapp locations, and (iii) locations of rib thermocouples.

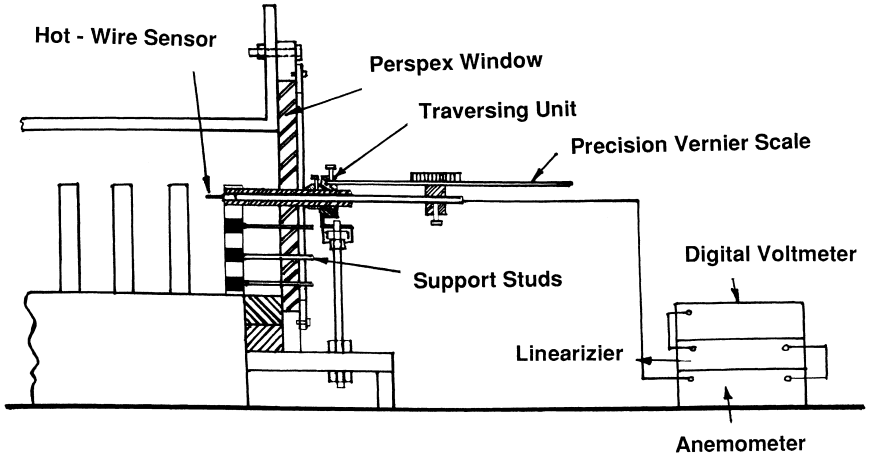

Fig. 3. Experimental set-up for local measurements.

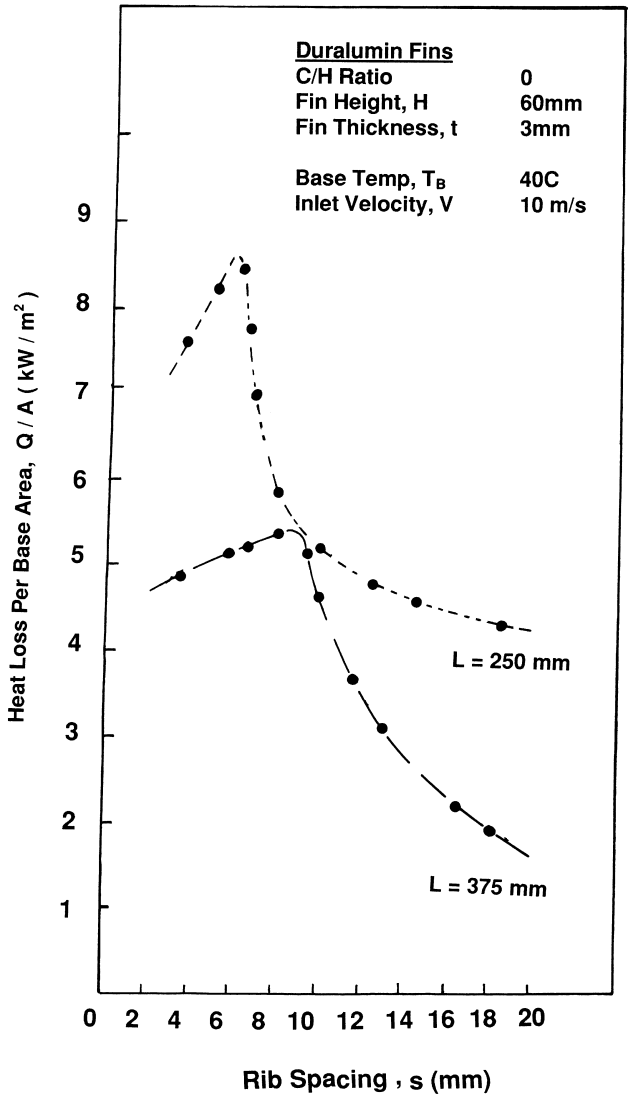

Fig. 4. Variation of heat transfer from longitudinal ribs with respect to rib spacing (Naik et al., 1988).

Although the effect of increasing the Reynolds number increased the heat transfer rate, this corresponded with only a small marginal reduction in the optimal spacing.

In this study, the optimal rib spacings obtained by Naik et al. (1988) have been correlated by regression analysis and for the geometrical conditions indicated in Table 1, it was found that the distribution of this optimal rib spacing can be expressed by,

$$\left(\frac{s_{\text{opt}}}{H}\right) = 0.0359\left(\frac{H}{L}\right)^{-0.642} \text{Re}^{0.023}, \tag{1}$$

which has a correlation coefficient of 0.9813 and is valid for $0.085 \leqslant H/L \leqslant 0.36$, $0.039 \leqslant s/H \leqslant 0.6$, $13 \leqslant L/s \leqslant 107$, $0 \leqslant C/H \leqslant 1$ and $3.1\times10^3 \leqslant \text{Re} \leqslant 3.4\times10^4$ when the Reynolds number is defined by,

$$\text{Re} = \frac{(m/A_{\text{ff}})D_{\text{e}}}{\mu}. \tag{2}$$

The hydraulic diameter, $D_{\text{e}} = 4A_{\text{ff}}/P$, is based on the free-flow area and the wetted perimeter of the ribs, spacer bars and the enclosing duct. The distribution of s_{opt} described by Eq. (1) is shown by Fig. 5 from which it is evident that the optimal rib spacing is independent of the C/H ratio and only weakly dependent on the Reynolds number.

The occurrence of the optimal rib spacing and the corresponding maximum rates of heat transfer from the rib array is attributed to conflicting processes which ensue between the heat transfer surface area of the array, the heat-transfer coefficient, the thermal boundary-layer formation on the heat-transfer surfaces, and the distribution of the bulk mean temperature within the rib spacings. For a constant mass flow through the test section, the effect of utilising narrow spacings will increase the number of ribs per unit width and hence augment the heat transfer surface area. Additionally lower bulk fluid temperatures also ensue within the rib channels. However, with higher rib spacings, higher bulk fluid temperatures and lower heat transfer surface areas result. Due to these interacting effects, the net result is a maximum in the value of the heat transfer from the ribs with respect to variations in s.

3.2. Comparison with pin fin turbulence promoters

In order to compare the level of heat transfer augmentation which can be achieved with longitudinal ribs, their average experimental Nusselt numbers have been compared with the heat transfer characteristics of an equivalent empty duct, circular pins, Metzger et al. (1984), and cubic and diamond pins, Chyu et al. (1996). For the empty equivalent duct, it has been assumed that the heat transfer can be described by the Dittus–Boettler correlation, Dittus and Boelter (1930), i.e

$$\text{Nu}_{D_{\text{h}}} = 0.023\,\text{Re}^{0.8}\,\text{Pr}^{0.4}, \tag{3}$$

in which Re is based on the hydraulic diameter of an equivalent empty duct and is valid for $6000 < \text{Re} < 10^7$. The heat transfers from cubic and diamond pins are represented by the correlations determined by Chyu et al. (1996) for a pin diameter to height ratio of unity, and center line to center line pin streamwise and transverse spacings of 2.5, i.e.

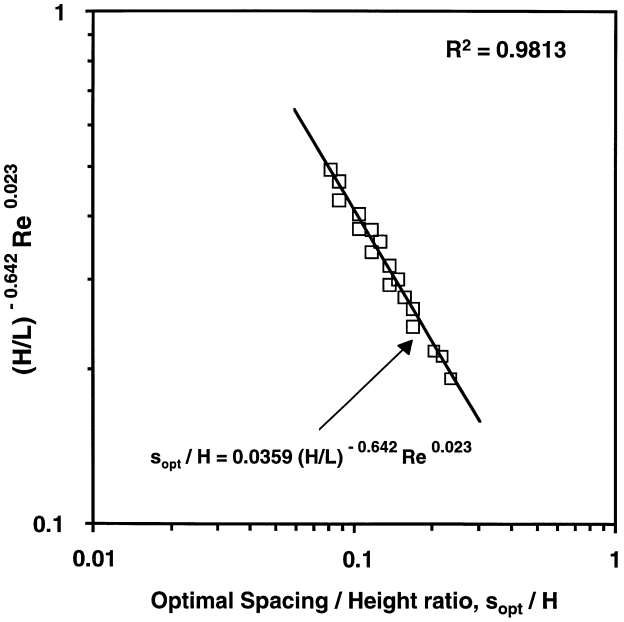

Fig. 5. Variation of optimal separation of longitudinal ribs corresponding to the maximum rate of heat transfer.

$$Nu_H = 0.138\,Re_H^{0.704}\,Pr^{0.4} \quad \text{(Staggered Cube Pins)}, \tag{4}$$

$$Nu_H = 0.084 Re_H^{0.732}\,Pr^{0.4} \quad \text{(Staggered Diamond Pins)}. \tag{5}$$

The heat transfer from circular pins, with pin diameter to height ratio of unity, and center line to center line pin streamwise and transverse spacings of 2.5, are represented by the experimental data of Metzger et al. (1984). The average heat transfer in longitudinal ribs, for the range of parameters indicated by Table 1 can be described by the correlation previously determined by Naik et al. (1988), i.e.

$$Nu_d = 0.273[Re]^{0.775}[s/L]^{0.680}[C/H]^{0.033}, \tag{6}$$

which is valid for $3.1 \times 10^3 \leqslant Re \leqslant 3.4 \times 10^4$, $9.33 \times 10^{-3} \leqslant s/L \leqslant 7.6 \times 10^{-2}$ and $0 \leqslant C/H \leqslant 1$. This correlation is accurate to within $\pm 15\%$, when the Nusselt number is defined by,

$$Nu_d = h_{av} D_h / k, \tag{7}$$

where the hydraulic diameter, $D_h = 4A_{ff} / P_h$, and P_h is the heated perimeter of the ribs and spacer bars surfaces. The fluid properties are based on the bulk fluid temperatures and the average heat transfer coefficient in Eq. (7) is based on the total heat transfer surface area, A_s, with the Reynolds number being described by Eq. (2). The average heat transfer characteristics of the longitudinal ribs described by Eq. (6) is illustrated in Fig. 6 with the measured experimental data. This shows that although Re and s/L strongly influence Nu_d, the C/H ratio exhibits only a weak effect. The latter is due to the interaction between the reduced heat transfer coefficient and increased hydraulic diameter as the C/H ratio is increased. And because Nu_d is directly proportional to the product $h_{av}D_h$, the above two effects tend to diminish the influence of the C/H ratio on Nu_d.

As the Nusselt and Reynolds numbers for the pin fins (Chyu et al., 1996; Metzger et al., 1984) are based on the pin diameter, for pin height/diameter ratio of unity, the Nusselt and Reynolds numbers for the longitudinal ribs have been re-evaluated and are based on the rib height in order to maintain consistent length scales. The thermal performances of all the considered pin fins and some of the longitudinal ribs are indicated by Fig. 7. It is evident from this figure, that at H/L ratios of 0.24 and 0.36, the Nusselt numbers are much higher for the longitudinal ribs compared to the staggered cubic and diamond pins examined by Chyu et al. (1996). These higher Nusselt number are achieved for the whole range for rib spacings examined, i.e. from $1.5 \leqslant s/t \leqslant 6.7$. Fig. 7 also shows that although the heat transfer performances of the longitudinal ribs decreases as the H/L ratio reduces to 0.13 and 0.08, they are still comparable to the pin fin turbulence promoters.

The thermal comparisons in Fig. 7 are only valid for pin height/diameter ratios of unity. However, Brigham and Van-Fossen (1984) have shown that variations in the pin fin Nusselt numbers are negligible for pin height/diameter ratios ranging from 1–2, whereas for 2 < pin height/diameter $\leqslant 8$, the pin fin Nusselt numbers increase significantly and are dependant on both the Reynolds number and the pin height/diameter ratio.

The frictional characteristics of the pin fins and the longitudinal ribs, are shown by Fig. 8 with respect to the Reynolds number. The Darcy friction factor is represented by,

$$f = \frac{2\rho\Delta P}{(L/D_e)(m/A_{ff})^2}, \tag{8}$$

in which ΔP is the total pressure drop across the whole rib array. For the above longitudinal ribs, friction factor correlations have been proposed by Naik et al. (1988), when $C/H = 0$ and $C/H = 0.5$. These correlations are, however, based only on the 'frictional' pressure drop within the ribbed array and do not account for the pressure drop at the rib array entrance and the pressure rise at the array exit.

The frictional characteristics of the smooth equivalent empty duct in Fig. 8 are represented for $3 \times 10^3 \leqslant Re \leqslant 3 \times 10^6$ by the Karman–Nikuradse correlation (Kays and Crawford, 1980),

$$f^{-1/2} = 2\log(Re\, f^{1/2}) - 0.8, \tag{9}$$

and the frictional losses for the pin fins are those based on the experimental data of Chyu et al. (1996) and Metzger et al. (1984). It is evident from Fig. 8 that the friction factors for the cubic and diamond pins are significantly higher than that of the circular pins, longitudinal ribs and the smooth equivalent duct. The frictional losses for the longitudinal ribs are, however, similar to that of the circular pins.

In addition to the average thermal-hydraulic performance comparisons between the pin fins and the longitudinal ribs, the volume and surface area requirements of the various heat

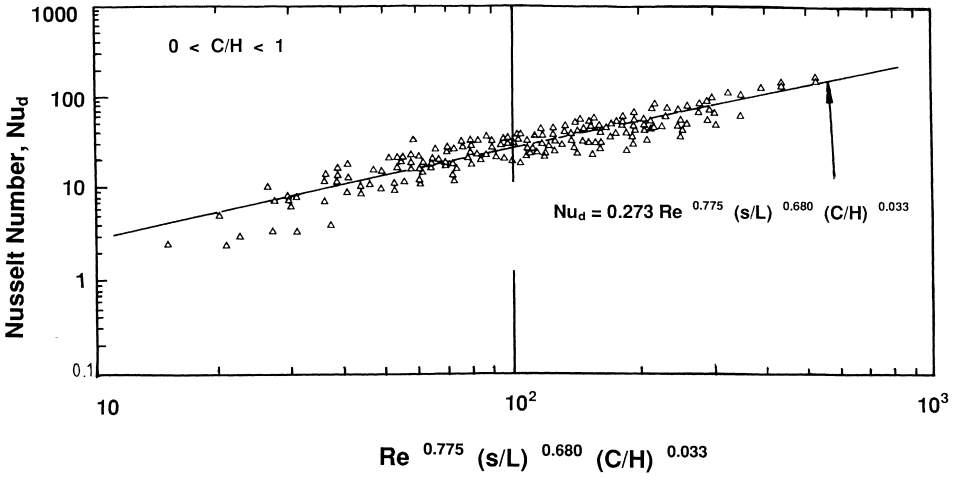

Fig. 6. Average thermal characteristics of longitudinal ribs (Naik et al., 1988).

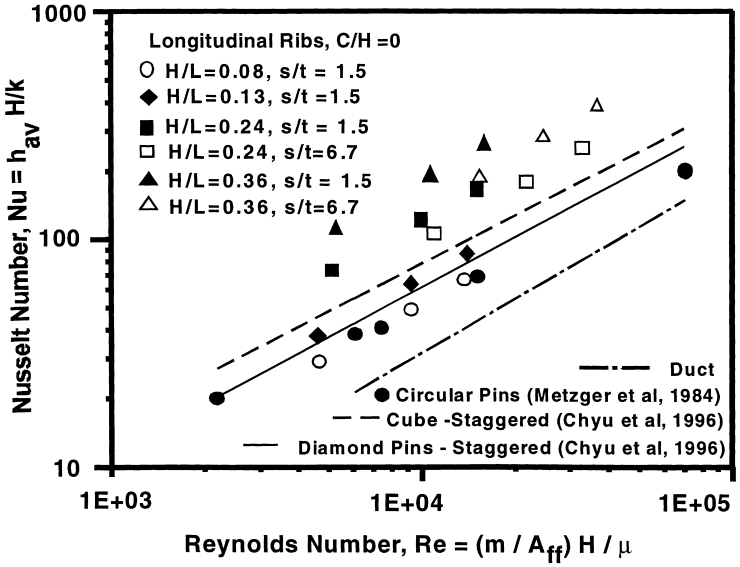

Fig. 7. Comparisons of the thermal characteristics of the longitudinal ribs and pin fins at $C/H = 0$.

transfer augmentation devices, have also been compared. Table 2 shows the variations of the volume (V_{vol}) and surface area (A_s) of the pin fins and the longitudinal ribs with respect to the volume (V^0_{vol}) and surface area (A_0) of an equivalent empty duct. The thickness of the longitudinal ribs used in the present study is 3 mm, whereas the diameter (or width) of the pin fins used by Chyu et al. (1996) is 12.5 mm. It is clear from Table 2, that, at low rib spacings, the volume (and hence weight) requirements for the ribs are, as expected, more than twice that of the pins, which is a considerable disadvantage for gas turbine applications despite the higher heat transfer rates. However, at high rib spacings, e.g. $s/t = 6.7$, the volume occupied by the ribs drops significantly, due to the lower number of ribs required per unit width of the duct, and attains values lower than those associated with the in-line and staggered pin fins. At these high rib spacings, Table 2 also shows that the surface area of the ribs is also more than nine times that of the pins. As indicated by Fig. 7, the Nusselt numbers of the ribs at these larger spacings are also higher than that associated with the pin fins.

For gas turbine blade cooling applications, it is clear from Figs. 7 and 8 and Table 2, that under conditions of high rib spacings and $H/L \geqslant 0.24$, the longitudinal ribs can offer better advantages in terms of both thermal-hydraulic performances and weight considerations, when compared with the cubic and diamond pin fin arrays.

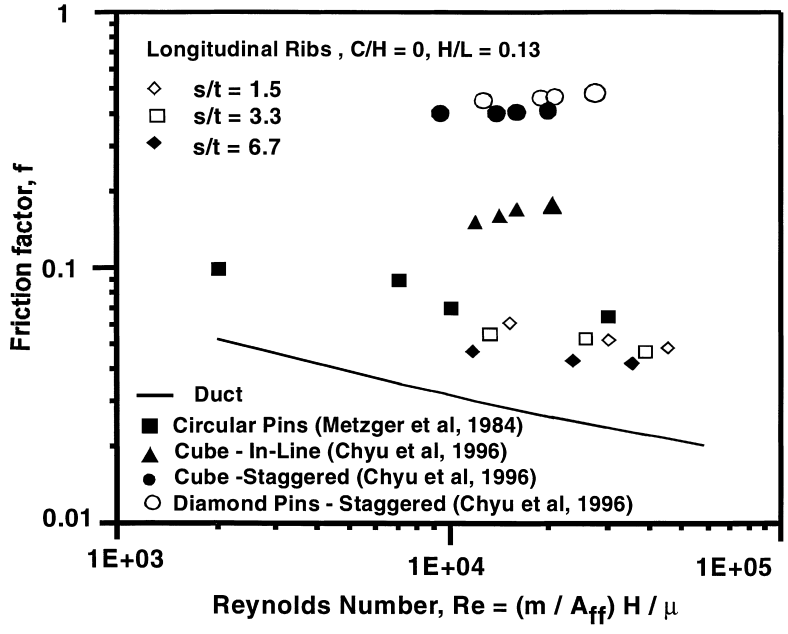

Fig. 8. Comparisons of the frictional characteristics of the longitudinal ribs and pin fins at $C/H = 0$.

Table 2
Variations in volume and surface areas of longitudinal ribs and pin fins

	Longitudinal ribs				Cubic/Diamond Pin Fins (Chyu et al., 1996)	
	$H/L=0.36$		$H/L=0.24$			
s/t	1.5	6.7	1.5	6.7	In-Line	Staggered
V_{vol}/V^0_{vol}	0.41	0.143	0.41	0.143	0.172	0.157
A_s/A_0	8.56	3.0	6.37	2.23	0.318	0.292

4. Local thermal-hydraulic characteristics

4.1. Local velocity profiles

The local velocity profiles within the rib channels were measured for two rib spacings, i.e. when $s=10$ mm ($s/t=3.33$) and $s=5$ mm ($s/t=1.67$) and when C/H is zero and 0.5. The rib height and length were 32 mm and 250 mm, respectively. The measured velocities are the time-averaged mean values and the maximum error of all the measured values was ±5%. The distributions are indicated by Figs. 9 and 10. For all the cases examined the Reynolds number (as defined by Eq. (2)) was maintained constant at 1.38×10^4.

When $C/H=0$, Fig. 9 shows the typical turbulent flow profile within the channel, and as expected, lower velocities ensue at the rib walls due to the wall friction, which then increase in magnitude as the channel center-line is approached. Comparisons of the velocity distribution in the streamwise direction from $z/L=0.5$–0.97 show that the mean velocities at every transverse location are varying in the streamwise direction, indicating hydrodynamic developing flow conditions within the rib channels

When $C/H=0.5$, Fig. 10 shows that most of flow is confined in the clearance gap above the ribs especially in the vicinity of rib walls. This is to be expected, as the clearance gap is the flow path of least resistance as the flow progresses through the test section. Along the rib height, the velocity increases quite significantly from the base of the ribs to its tip, particularly at locations very near the rib wall. However along the center-line of the channel the velocity profile is fairly constant within the rib channel and in the clearance gap. It is also clear from Fig. 10, that when $C/H=0.5$, the changes in the profile and magnitude of the mean velocity which ensue in the stream wise direction from $z/L=0.5$–0.97, are indicative that hydrodynamic developing flow conditions are present within the rib channels.

4.2. Local heat-transfer coefficients

In order to evaluate the local heat transfer coefficients along the rib height and length, the local fluid temperatures were measured within the complete cross-sectional area of the channel at streamwise locations $z/L=0.5$ and $z/L=0.97$. The temperature of the solid rib surfaces were measured with embedded thermocouples within the high conductivity duralumin ribs. Special care was taken to determine the local fluid temperatures in the vicinity of the rib walls where fluid temperature measurements were made within the expected thickness of the laminar sub-layer zone. In this study, it has been assumed that the temperature distribution within this conduction sublayer can be described empirically (Kays and Crawford, 1980) by

$$T^+=\mathrm{Pr}\eta^+ \quad \text{when} \quad \eta^+\leqslant 13.2, \tag{10}$$

which is based on Prandtl's mixing length hypothesis and in which the normal non-dimensionalised distance from the wall defining the conduction sub-layer is $\eta^+\leqslant 13.2$. Under this assumption, the normal distance corresponding to the conduction sub-layer in the present study would be 0.25 mm for the considered ranges of the Reynolds number.

Initially the temperature gradient $\mathrm{d}T/\mathrm{d}x$ within the conduction sub-layer was determined from measurements of the local fluid temperature at normal distances of 0.15 mm and 0.25 mm from the rib wall (i.e. along the x-coordinates in Fig. 2 (iii) with the probe inserted as indicated in Fig. 3) and at several locations along the rib height (ranging from $0.15\leqslant y/H\leqslant 0.85$) when $z/L=0.5$. It was found that, for all the test

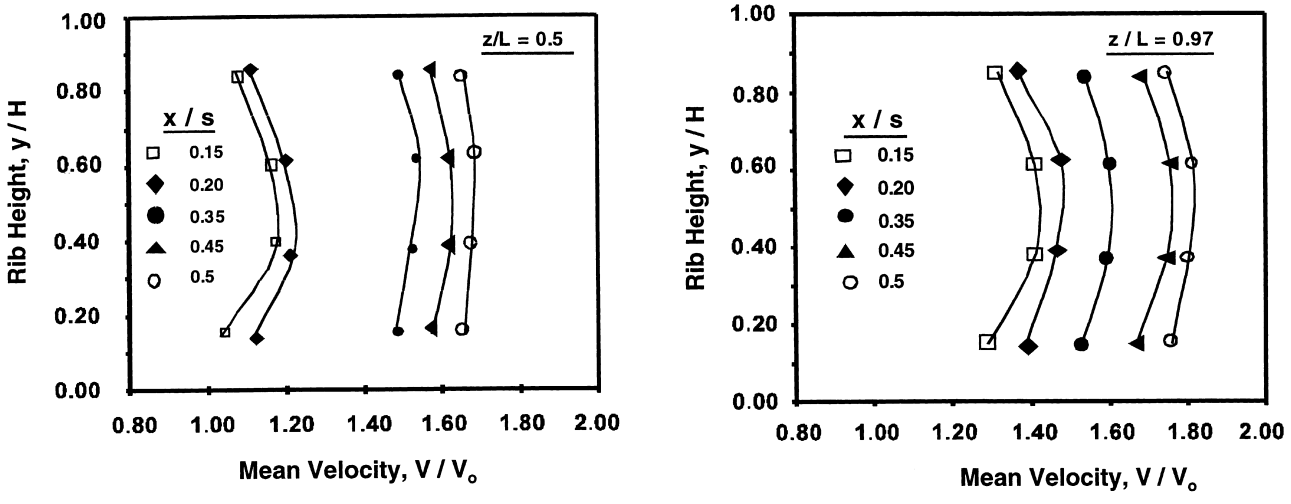

Fig. 9. Local velocities in rib channel when $C/H=0$, $s/t=3.3$, $H/L=0.13$, $\mathrm{Re}=1.38\times10^4$ at (a) $z/L=0.5$, (b) $z/L=0.97$.

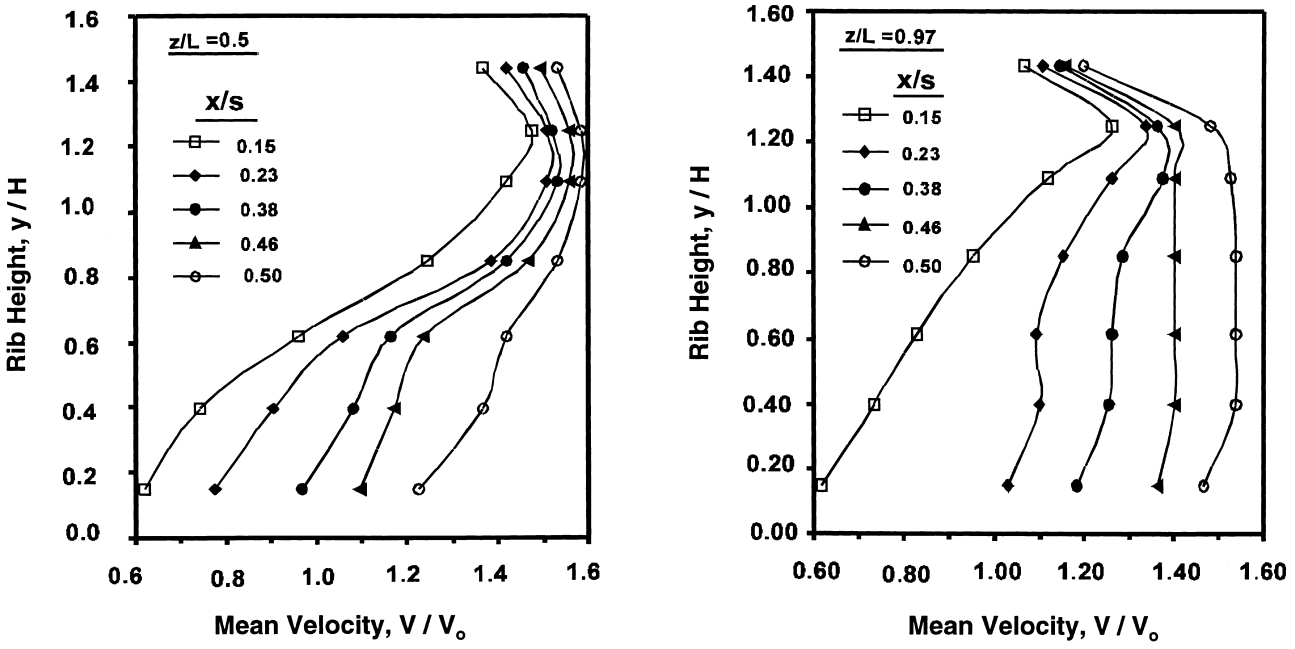

Fig. 10. Local velocities in rib channel when $C/H = 0.5$, $s/t = 3.33$, $H/L = 0.13$, $\mathrm{Re} = 1.38 \times 10^4$ at (a) $z/L = 0.5$, (b) $z/L = 0.97$.

undertaken, the differences in the temperature gradient at these two normal locations were less than 5% and in the regions halfway along the rib height, these differences diminished to less than 2%. The temperature gradient within the sub-layer was hence based on the air temperature measurements undertaken at a normal distance of 0.15 mm from the wall and the local heat transfer coefficient then determined from,

$$h(y) = \frac{K\left[\frac{\mathrm{d}T}{\mathrm{d}x}\right]_{x \leqslant \eta^+, y}}{(T_\mathrm{b} - T_\mathrm{bulk})}, \tag{11}$$

where,

$$T_\mathrm{bulk} = \frac{1}{V_\mathrm{bulk}[(s+t)\ (C+H) - Ht]} \int\int TV\ \mathrm{d}x\mathrm{d}y \tag{12}$$

and,

$$V_\mathrm{bulk} = \frac{1}{[(s+t)\ (C+H) - Ht]} \int\int V\ \mathrm{d}x\mathrm{d}y. \tag{13}$$

The temperature differential, $\mathrm{d}T$, in Eq. (11) is that corresponding to the difference between the solid rib surface and the fluid temperatures within the conduction sub-layer, and the local heat transfer coefficient is based on the rib base temperature, T_b. The errors in the measurements of h are indicated

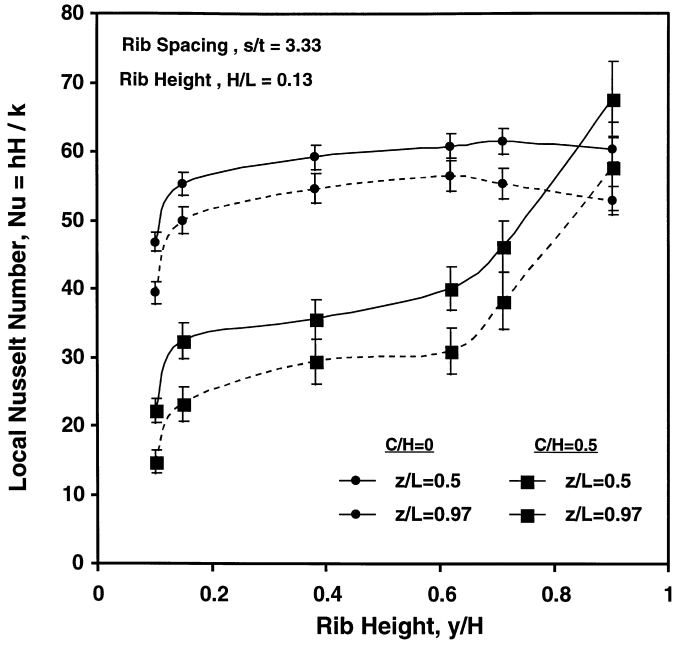

Fig. 11. Variation of the rib local Nusselt numbers at $s/t = 1.67$, $H/L = 0.13$ and $\mathrm{Re} = 1.38 \times 10^4$.

in Figs. 11 and 12 and are primarily associated in the measurement of dT/dx.

The distributions of the local Nusselt numbers (based on rib height and h) along the rib height for the two rib spacings considered are shown by Figs. 11 and 12. In general, it was observed that the local Nusselt number is non-uniform along the rib height for all the cases considered. At $C/H=0$, this non-uniform distribution of Nu is due to a combination of factors which include, the variation in the velocity profile at the rib wall, the different thermal boundary conditions at the base of the ribs and that at the roof of the duct and the temperature gradient in the solid rib along its height. The variation in the velocity profile results in parts of the rib adjacent to the base and the shroud to be washed by a relatively low-velocity air. This results in higher air temperatures in these regions compared with those prevailing within the central region of the rib height, which is subjected to a higher velocity fluid. The effect of a constant temperature boundary condition at the base of the ribs also results in higher fluid temperatures in the conduction sub-layer and thereby lower heat transfer coefficients. And, at the roof of the duct, which is adiabatic, the fluid temperature in the conduction sub-layer near the rib tip are much lower than that at its base resulting in relatively higher values of the local heat transfer coefficient.

Figs. 11 and 12 also show that there are no significant differences in the local Nu due to changes in the rib spacing, particularly at $C/H=0$. Although at constant Reynolds number, lower bulk fluid temperatures and higher temperature gradients ensue within the conduction sub-layer with the narrowly spaced ribs, the bulk fluid temperatures are higher at the higher rib spacing with correspondingly lower temperature gradients in the boundary layers. Due to these effects Figs. 11 and 12 indicate relatively modest variations in Nu due to changes in the rib spacing. Figs. 11 and 12 also show that Nu reduces in the streamwise direction along the rib channel for both the rib spacings considered, indicating that thermally developing flow conditions are prevalent.

When there is a clearance gap above the ribs, Figs. 11 and 12 illustrate that the local Nusselt numbers along most of the rib height are much smaller than that corresponding to $C/H=0$. This is because the local velocities within the rib channels are lower when compared to $C/H=0$. This consequently result in higher bulk fluid temperatures and lower temperature gradients within the boundary layers at the rib surfaces. However, as the tip of the rib is approached, the local Nu begins to increase and attains its highest value at the rib tip. This is to be expected, because very high velocities ensue in this region which results in lower air temperatures at the rib tip. Although there is also a decreasing temperature gradient within the solid rib along the rib height, its influence on the local heat transfer coefficient is relatively small compared with that due to the lower bulk fluid temperatures within the rib channels.

When $C/H=0.5$, Figs. 11 and 12 also show that the local Nusselt numbers reduce as the flow progresses down the length of the rib channel. This is indicative that thermally developing flow conditions also exist within the rib channels at $C/H=0.5$.

5. Conclusions

The optimal separation of longitudinal ribs which corresponded to the maximum rate of heat transfer from longitudinal rib arrays were collated from a previous study, for a range of rib heights, lengths and the magnitude of the clearance gap above them. In this study it has been found that this optimal rib separation can be described empirically by

$$\left(\frac{s_{\text{opt}}}{H}\right)=0.0359\left(\frac{H}{L}\right)^{-0.642}\text{Re}^{0.023},$$

which has a correlation coefficient of 0.9813 and is valid for $0.085\leqslant H/L\leqslant 0.36$, $0.039\leqslant s/H\leqslant 0.6$, $13\leqslant L/s\leqslant 107$, $0\leqslant C/H\leqslant 1$ and $3.1\times 10^3\leqslant \text{Re}\leqslant 3.4\times 10^4$. Overall, the tall ribs yielded greater rates of heat transfer and higher optimal rib spacings, whereas the long ribs resulted in smaller heat transfer rates but higher optimal rib spacings.

Comparisons of the thermal performances of longitudinal ribs with those of circular, cubic and diamond pins indicate that under certain geometrical conditions, longitudinal ribs can provide higher heat transfer rates and lower volume

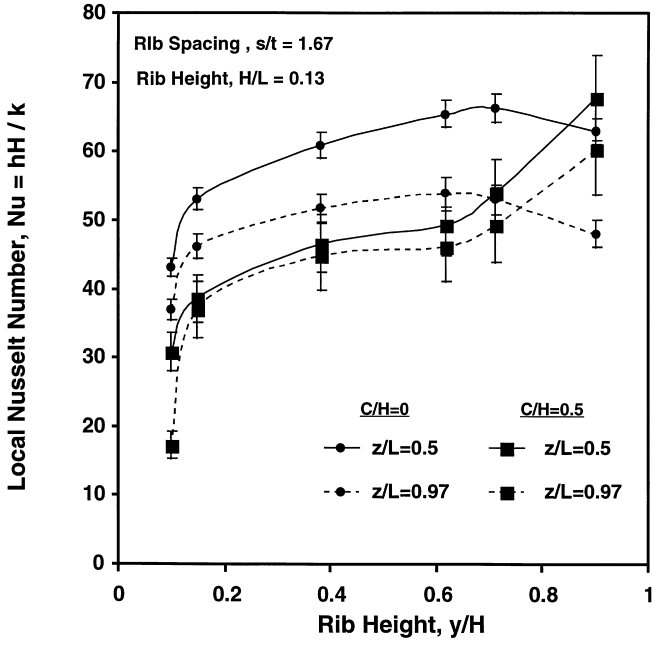

Fig. 12. Variation of the rib local Nusselt numbers when $s/t=3.33$, $H/L=0.13$ and $\text{Re}=1.38\times 10^4$.

requirements compared with pin fin configurations. The hydraulic performance of the longitudinal ribs was found to be similar to that of the circular pin fins considered in this investigation.

Detailed local measurements of mean velocities and temperatures within the rib channels indicated that developing flow conditions existed within the rib configurations considered in this study. The effect of introducing clearance gaps above the ribs, forced most the incoming flow to be within this clearance particularly in the vicinity of the ribs. However, within the central symmetrical section of the channels, a near uniform velocity profile results along the height of the ribs and within the clearance gap.

The local heat transfer coefficient distribution along the height of the ribs for a limited range of geometries indicated that its magnitude and profile was highly influenced by the amount of clearance above the ribs. Lower heat transfer coefficients ensue when a clearance gap is introduced above the ribs which varies from an almost constant value along most of the rib height to a maximum value at the tip of the rib.

References

Babus'haq, R.K., Akintunde, K., Probert, S.D., 1995. Thermal performance of a pin-fin assembly. Int. J. Heat and Fluid Flow 16 (1), 50–56.

Bejan, A., Sciubba, E., 1992. The optimal spacing of parallel plates cooled by forced convection. Int. J. Heat. Mass. Transfer 35 (12), 3259–3264.

Brigham, B.A., VanFossen, G.J., 1984. Length to diameter ratio and row effects number in short pin fin heat transfer. J. Eng. Gas Turbines and Power 106, 241–245.

Chyu, M.K., Hsing, Y.C., Natarajan, V, 1996. Convective Heat Transfer of cubic fin arrays in a narrow channel. 41st Int Gas Turbine and Aeroengine Congress, Birmingham, UK, 3–5 June, Paper No. 96-GT-201.

Chyu, M.K., 1990. Heat transfer and pressure drop for short pin-fin arrays with endwall heat transfer. J. Heat Transfer 112, 926–932.

Dittus, F.W., Boelter, L.M.K., 1930. Univ of Calif. Berkeley Publ. Eng 2, 443.

Han, J.C., Zhang, Y.M., 1992. High performance heat transfer ducts with parallel broken and V-shaped broken ribs. In. J. Heat. Mass. Transfer 35 (2), 513–523.

Han, J.C., Park, J.S., Lei, C.K., 1985. Heat Transfer enhancement in channels with turbulence promoters. J. Engrg. for Gas Turbines and Power 107, 628–635.

Hishida, M., 1996. Local heat transfer coefficient distribution on a ribbed surface. J. Enhanced Heat Transfer 3 (3), 187–200.

Kadle, D.S., Sparrow, E.M., 1986. Numerical and experimental study of heat transfer and fluid flow in longitudinal fin arrays. ASME J Heat Transfer 108, 16–23.

Kays, W.M., Crawford, M.E., 1980. Convective Heat and Mass transfer, 2nd ed. McGraw-Hill.

Knight, R.W., Goodling, J.S., Hall, D.J., 1991. Optimal thermal design of forced convection heat sinks - Analytical. J. Electronic Pack 113, 313–321.

Leung, C.W., Probert, S.D., Shilston, M.J., 1987. Heat exchnagers: Optimal separation for vertical rectangular fins protruding from a vertical rectangular base. Applied Energy 19, 77–85.

Kline, S.J., McClintock, F.A., 1958. Describing uncertainties in a single-sample experiments. ASME Mech Engng 3–8.

Metzger, D.E., Fan, C.S., Haley, S.W., 1984. Effects of pin shape and array orientation on heat transfer and pressure loss in pin fin arrays. J. Engrg. for Gas Turbines and Power 106, 252–257.

Minakami, K., Iwasaki, H., Mochizuki, S., Marata, A., Yagi, Y., 1994. Heat transfer characteristics of pin-fins with in-line arrangement. Heat Transfer–Japanese Research 23 (3), 213.

Moffat, R.J., 1988. Describing the uncertainties in experimental results. Exp Thermal Fluid Sci 1, 3–17.

Naik, S., Probert, S.D., Wood, C.I., 1988. Thermal-Hydraulic characteristics of a heat-exchanger: - The vertical fins being aligned to the mean air-flow in the duct. Applied Energy 29, 217–252.

Naik, S., Probert, S.D., Shilston, M.J., 1987a. Forced convective steady-state heat transfers from shrouded vertical fin arrays. Applied Energy 26, 137–158.

Naik, S., Probert, S.D., Wood, C.I., 1987b. Natural convection characteristics of a horizontally based vertical rectangular fin-array in the presence of a shroud. Applied Energy 28, 295–319.

Rau, G., Cakan, M., Moeller, D., Arts, T., 1996. The effect of periodic ribs on the local aerodynamic and heat transfer performance of a straight cooling duct. 41st Int Gas Turbine and Aeroengine Congress, Birmingham, UK 3–5 June, Paper No. 96-GT-541.

Sparrow, E.M., Baliga, B.R., Patankar, S.V., 1978. Forced convection heat transfer from a shrouded fin-array with and without tip clearance. ASME J. Heat Transfer 100, 572.

Sparrow, E.M., Beckley, T.J., 1981. Pressure-drop characteristics for a shrouded rectangular fin array with tip-clearance. ASME J Heat Transfer 103, 393.

Thombre, S.B., Sukhatme, S., 1995. Turbulent flow heat transfer and friction factor characteristics of shrouded fin arrays with uninterrupted fins. Exp. Thermal and Fluid Sci 10 (3), 388–402.

VanFossen, G.J., 1982. Heat Transfer coefficients for staggered arrays of short pin fins. J. Engng. for Power 104, 268–274.